Type of the Paper (Article, Review, Communication, etc.)

Studies of fracture damage caused by proppant embedment phenomenon in shale rock

Mateusz Masłowski *, Piotr Kasza, Marek Czupski, Klaudia Wilk and Rafał Moska

Oil and Gas Institute – National Research Institute, Lubicz 25A Str., 31-503 Cracow, Poland; office@inig.pl
* Correspondence: Oil and Gas Institute – National Research Institute, Armii Krajowej 3 Str., 38-400 Krosno, Poland; mateusz.maslowski@inig.pl

Received: date; Accepted: date; Published: date

The result of laboratory imaging of the embedment phenomenon may be one of the preliminary assessment of the effectiveness of hydraulic fracturing at the design stage.

Abstract: This paper concerns the effect of proppant embedment related with hydraulic fracturing treatment. This phenomenon occurs if the strength of the reservoir rock is lower than proppant grains. The aim of the research is laboratory determining the loss of width of the proppant pack built of light ceramic grains. The laboratory simulation of the embedment phenomenon was carried out for a shale rock on a hydraulic press, in a specially prepared for this purpose a heated embedment chamber. Tests were conducted at high temperature and axial compressive stress conditions. The surfaces of the cylindrical core plugs (fracture faces) were imaged under an optical microscope equipped with 3D software. The fracture faces were examined and compared before and after the embedment phenomenon. The analysis of the obtained images of the fracture face were made based on the research method of the embedment phenomenon developed at Oil and Gas Institute-NRI. On the basis of laboratory tests, the parameters characterizing the embedment phenomenon were collected and discussed. In addition, the percentage reduction in the width of the proppant pack was determined.

Keywords: embedment; shale rock; proppant pack; fracture width

1. Introduction

Hydraulic fracturing is one of the main methods for stimulating unconventional hydrocarbon reservoirs. In the case of shale foramtions, which are characterized by increased content of clay minerals, for intensification treatments to be effective, numerous fractures and cracks should be created in them [1-7], as shown in Figure 1 [2,8,9,10].

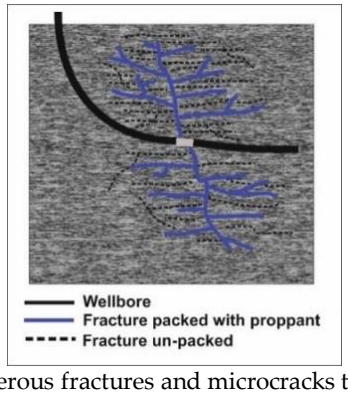

Figure 1. Visualization of numerous fractures and microcracks that allow the gas absorbed to release from the shale rock.

Peer-reviewed version available at Appl. Sci. 2019, 9, 2190; doi:10.3390/app9112190

Numerous fractures and cracks created in shale formations are characterized by low width and large values of the stimulated reservoir volume (SRV). It also has to be pointed out that proper selection of proppant should ensure high conductivity of the whole generated system of fractures and placing proppant in the furthest parts of the fractures [11-13]. Apart of the way of transporting and placing proppant in the fracture, the phenomena presented in Figure 2 have a significant influence on its effective packed with proppant [10,13]. They occur after the treatment when the formation compressive stress closes the fracture on the proppant.

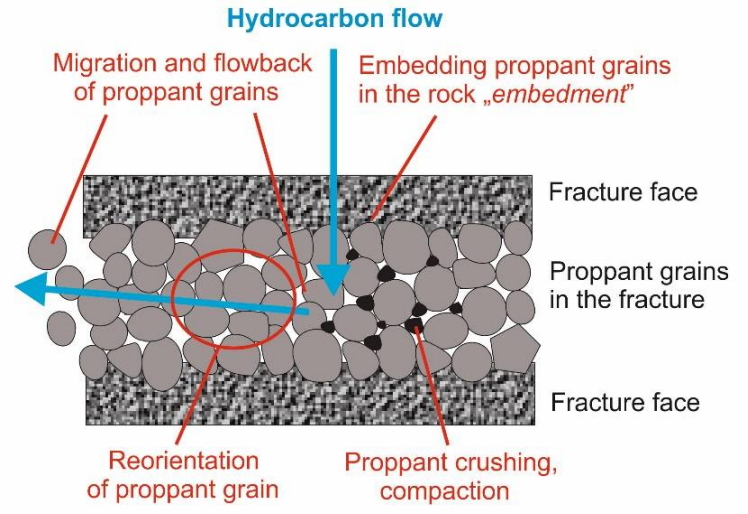

Figure 2. The phenomena influencing the effective packed of the fracture and achieving a high conductivity.

The geometric ideal model of the proppant embedment phenomenon is shown in Figure 3 [15,16].

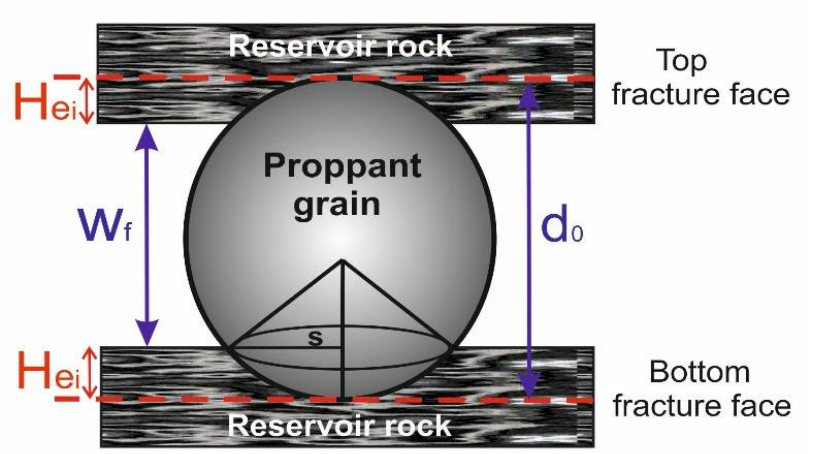

Figure 3. Geometric ideal model of the proppant embedment phenomenon.

The presented model of the proppant embedment phenomenon effects on decrease the width W_f of the created fracture (Figure 4) [7,10,17-20] and an increase in the damage of the fracture face, which results in a decrease of its permeability and conductivity [16, 21-23].

Peer-reviewed version available at Appl. Sci. 2019, 9, 2190; doi:10.3390/app9112190

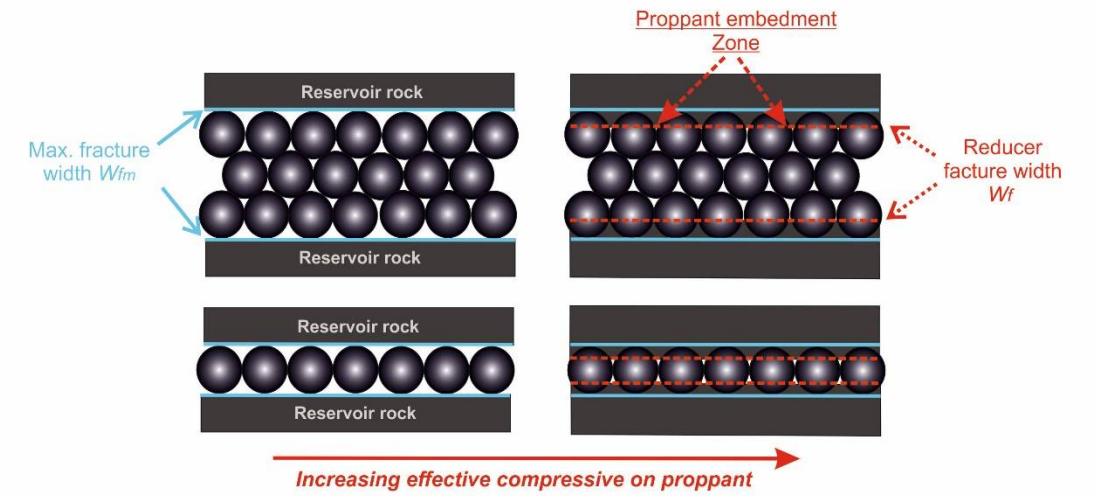

Figure 4. The effect of embedment phenomenon on the width of the packed fracture, for various proppant surface concentration.

For many years now, a number of laboratory tests, imaging tests and mathematical modeling of the embedment phenomenon have been undertaken. They are constantly being modernized as the capabilities of hardware and software are increasing.

2. Materials and Methods

2.1. Characteristics of the reservoir rock and proppant material used for testing

Shale rock (Figure 5.a) containing in its mineralogical composition 47.7% of clay minerals was used for testing. The content of quartz amounted to 24.4%, carbonates 14.2 % and others 13.7%. A lightweight ceramic proppant 30/50 mesh (Figure 5.b) with a grain size of 0.600÷0.300 mm was used as a proppant material.

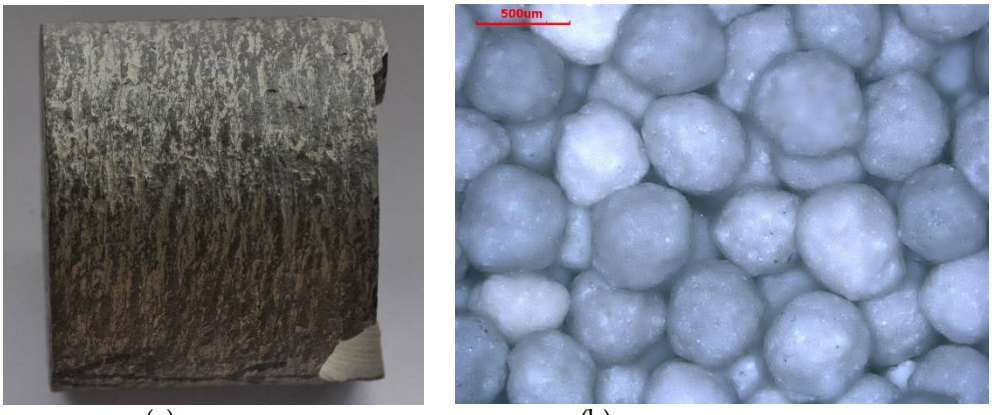

(a) (b)

Figure 5. Materials used for testing: a) Shale rock; b) Proppant

2.2. Methodology of studying the embedment phenomenon

The research methodology developed in Oil and Gas Institute – NRI was used [7,10,19,20,24]. It is an initial determination of primary roughness of the fracture face. It is determined for several selected areas, and then an average roughness is calculated for all of them, from the roughness profiles along the selected measurement sections. The method of determination of the surface roughness along the given measurement section is presented in Figure 6 [7,10,19,20], as well as using equation (1) [7,10,19,20,24].

Peer-reviewed version available at Appl. Sci. 2019, 9, 2190; doi:10.3390/app9112190

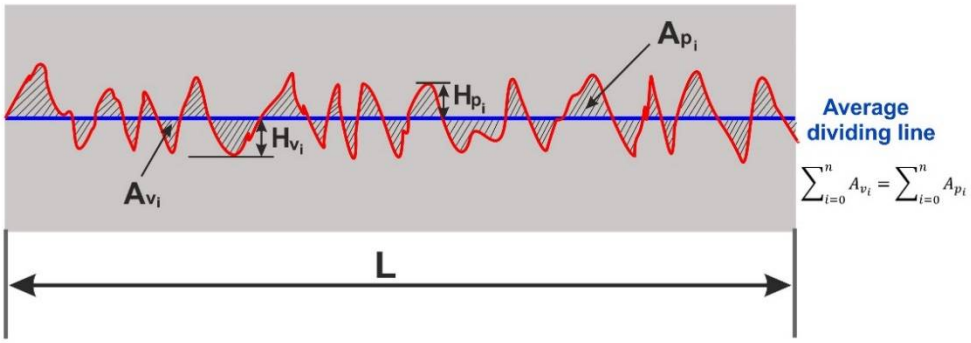

Figure 6. An example of the surface roughness profile along the measurement section for the selected area, on the surface of the fracture face.

$$R = \frac{\sum_{i=0}^{n} H_{p_i} + \sum_{i=0}^{n} H_{v_i}}{n_p + n_v} \quad (1)$$

Where R is roughness of the profile surface along the measurement section (mm); H_p is peak height (mm); H_v is valley depth (mm); n_p is number of all peaks (-); n_v is number of all valleys (-).

The average primary roughness R_a for the entire surface of the fracture face is determined as an arithmetic average of roughness of profiles determined for the individually selected areas.
Laboratory simulation of the embedment phenomenon consists in placing a proppant between two cylindrical core plugs, and then exposing it to the set axial compression stress, in the set temperature, for the set period of time (Figure 9.a and 9.b) [7,10,19,20].
The amount of the proppant material needed to pack the fracture and obtain the specified surface concentration is determined according to equation (2) [10,24,26].

$$m_p = A_f \cdot 10^{-1} \cdot C \quad (2)$$

Where m_p is weight of the proppant (g); C is surface concentration of the proppant (kg/m^2); A_f is surface area of the fracture face subjected to compression stress (cm^2).

The analysis of the fracture face after simulation of the embedment phenomenon consists in determination of an average depth of embedment of proppant grains as well as the damage of its surface. The method of determination of the embedment depth and the damage of the fracture face along the measurement section are presented in Figure 7 [7,10,19,20,25] and in the equation (3) [7,10,19,20,24].

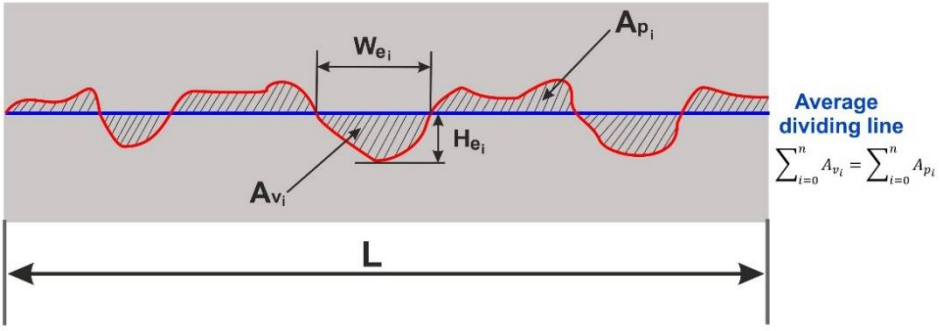

Figure 7. Sample profile of depth and width of grains embedment (valleys) along the measurement section for the selected area, on the surface of the fracture face.

Peer-reviewed version available at Appl. Sci. 2019, 9, 2190; doi:10.3390/app9112190

$$H_e = \frac{\sum_{i=0}^{n} He_i}{n_e} \quad (3)$$

Where He is average depth of proppant embedment in the fracture face of the profile, along the measurement section (mm); He_i is valley depth (embedment of a proppant grain in the fracture face) (mm); n_e is amount of all valleys (embedment of proppant grains in the fracture face) (-).

Total average depth He_t of proppant embedment in the fracture faces (rock), expressed in mm, is determined according to equation (4) [7,10,19,20,24].

$$H_{e_t} = H_{e_{T.a}} + H_{e_{B.a}} \quad (4)$$

Where $He._{T.a}$ is average depth of proppant embedment in the top fracture face, corresponding to arithmetic average of the obtained values for individually specified areas (mm); $He._{B.a}$ is average depth of proppant embedment in the bottom fracture face, corresponding to arithmetic average of the obtained values for individually specified areas (mm).

Percentage damage of the fracture surface PDW_e for the profile, along the measurement section is determined according to equation (5) [7,10,19,20], expressed in (%).

$$PDW_e = \frac{\sum_{i=0}^{n} We_i}{L} \cdot 100 \quad (5)$$

Where We_i is valley width, i.e. embedment of a proppant grain in the fracture face (mm); L is length of the measurement section (mm).

Total percentage damage of the fracture surface $PDWe_t$ (embedment of the embedding proppant grains on the surface of the fracture faces) is determined according to equation (6) [7,10,19,20], expressed in (%).

$$PDW_{e_t} = \frac{PDW_{e_{T.a}} + PDW_{e_{B.a}}}{2} \quad (6)$$

Where $PDW_{e_{T.a}}$ is average percentage damage of the surface of the top fracture face (rock), corresponding to arithmetic average of the obtained values for individually specified areas (%); $PDW_{e_{B.a}}$ is average percentage damage of the surface of the bottom fracture face (rock), corresponding to arithmetic average of the obtained values for individually specified areas (%).

The effect of the embedment phenomenon on the effective width of the fracture packed with proppant after exposure to axial compression stress is determined using equations (7) and (8) [7,10,19,20,24].

$$W_f = W_{f_m} - H_{e_t} \quad (7)$$

Where W_f is fracture width packed with proppant, taking into account the embedment phenomenon (mm); W_{fm} is maximum fracture width packed with proppant, without the occurrence of the embedment phenomenon (mm).

The percentage reduction of the fracture width PRW_f packed with proppant, taking into account the embedment phenomenon is determined according to equation (8) [7,10,19,20], expressed in (%).

Peer-reviewed version available at Appl. Sci. 2019, 9, 2190; doi:10.3390/app9112190

$$PRW_f = \frac{H_{e_t}}{W_{f_m}} \cdot 100 \quad (8)$$

The maximum width W_{fm} of the fracture packed with proppant, without the occurrence of the embedment phenomenon, is determined according to the research procedure previously mentioned in this paper. It only differs in the use of cylindrical steel plugs instead of cylindrical core plugs. They have a steel hardness of more than 43 on the Rockwell C scale (HRC). A maximum width W_{fm} of the fracture packed with proppant was being measured throughout the testing with the use of LVDT device. LVDT readings take into account the amount of deformation of the test unit (i.e. hydraulic press, measuring chamber and steel plugs) under the specified conditions of axial compressive stress and temperature.

3. Execution and analysis of obtained test results of laboratory simulation of the embedment phenomenon

The tests were performed on cylindrical core plugs with a diameter of 2.54 cm. First of all, the average primary roughness Ra for the entire surface of the core plug face (for the top and bottom fracture face), presented in Figure 8, was determined according to the test procedure described in the previous part of the paper. It was determined as an arithmetic average of two selected areas on the face of the tested core plug, from one profile running across the tested area. These tests were performed using an optical microscope, presented in Figure 9.c.

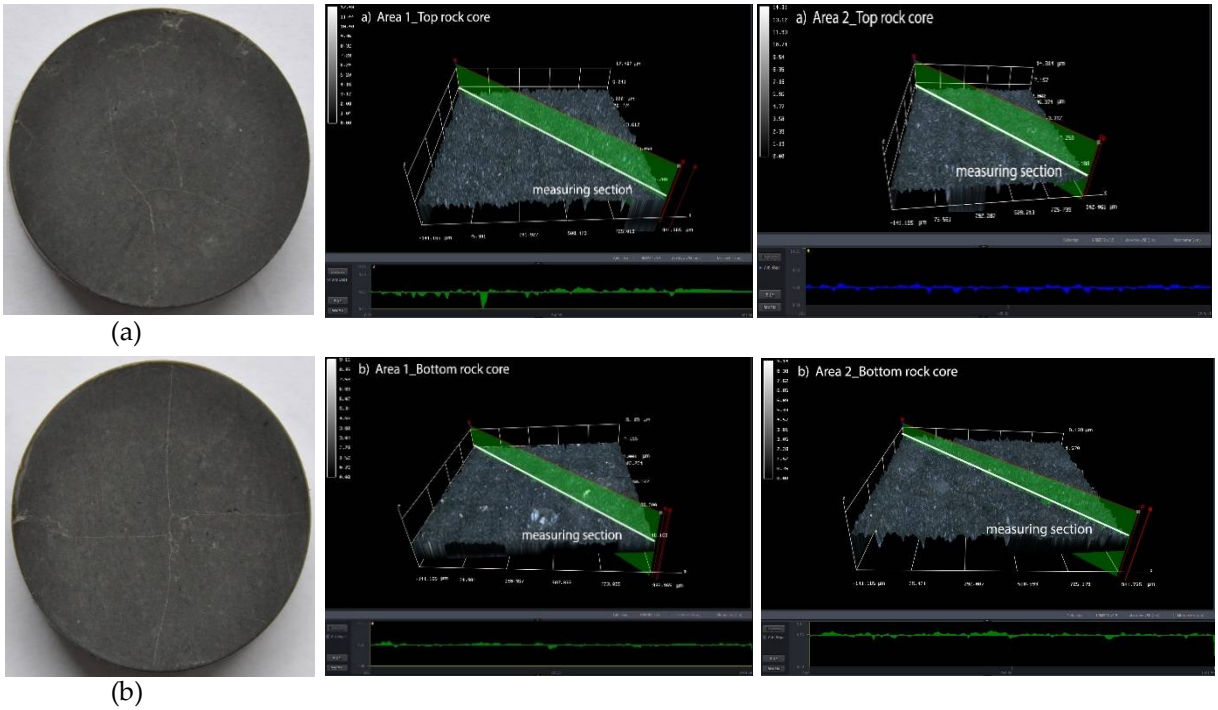

Figure 8. Determination of the primary roughness for the core plug face (fracture faces): (a) Top; (b) Bottom

The average primary roughness R_a for the entire face of the top core plug amounted to 0.00066 mm (+/- 0.00015 mm). For the bottom core plug it amounted to 0.00033 mm (+/- 0.00007 mm).

Next, laboratory simulation of the phenomenon of proppant embedment in the fracture faces, on the test unit presented in Figure 9 was carried out.

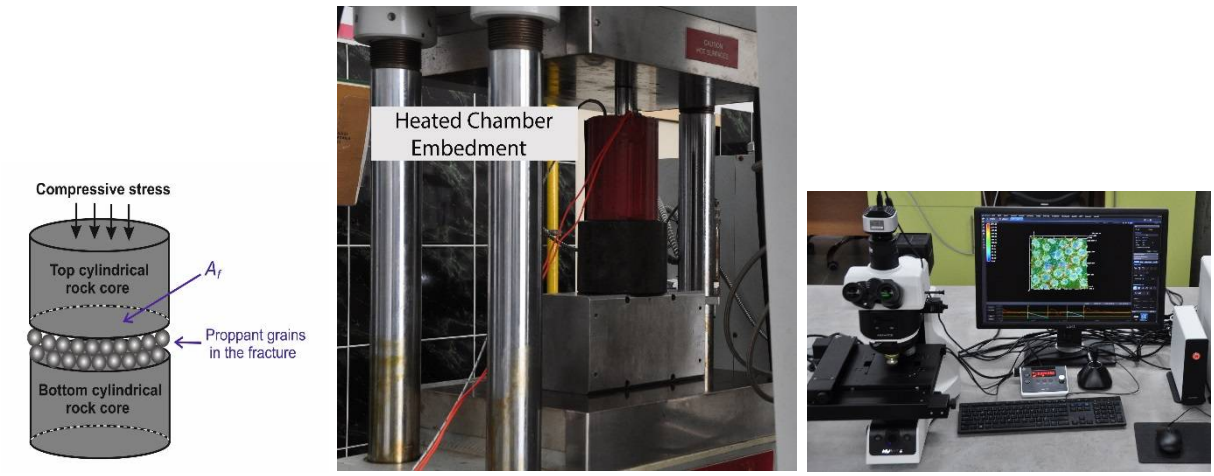

(a) (b) (c)

Figure 9. Test unit: (b) Hydraulic press with heating chamber for the simulation of embedment phenomenon; (c) Optical microscope with 3D software.

The test conditions are presented in Table 1.

Table. 1. Conditions for the test no. 1 and 2

Conditions for test	
Temperature, (°C)	70.0
Surface concentration of proppant, (kg/m²)	2.44
Compressive stress, (MPa)	48.3
Exposure to the defined compressive stress, (hours)	6

The result of test no. 1 is presented in Figure 10, 11, 12, 13, 14 and in Table 2, 3.

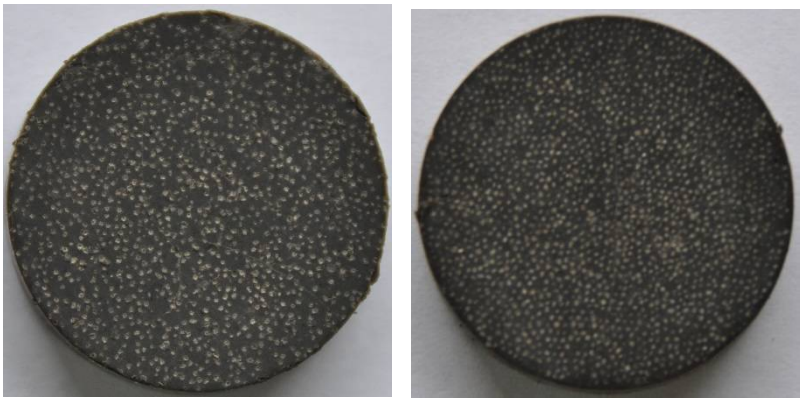

(a) (b)

Figure 10. Surface of the core plug sample at diameter 2,54 cm after embedment test: (a) Top; (b) Bottom.

Peer-reviewed version available at Appl. Sci. 2019, 9, 2190; doi:10.3390/app9112190

331 **Table 2.** Total average depth of proppant embedment in the fracture faces – Test 1

Fracture face	No. of the tested area	Surface area (mm^2)	Average measurement section length (mm)	Total measurement sections length (mm)	H_e (mm)	He_a (mm)	He_t (mm)
Top	**1**	7.2188	2.8230	11.2919	0.0141	0.0170	**0.0254**
	2	6.8904	2.6717	10.6866	0.0200		
Bottom	**1**	6.8251	2.6658	10.6632	0.0065	0.0084	
	2	6.9765	2.6620	10.6481	0.0102		

332
333
334 **Table. 3.** Average percentage damage of the fracture surface – Test 1

Fracture face	No. of the tested area	W_e (mm)	PDW_e (%)	$PDWe_a$ (%)	$PDWe_t$ (%)
Top	**1**	1.9268	17.1	19.2	**17.1**
	2	2.2712	21.2		
Bottom	**1**	1.5250	14.3	14.9	
	2	1.6647	15.6		

335
336
337
338
339
340
341
342
343
344
345
346
347
348

Preprints (www.preprints.org) | NOT PEER-REVIEWED | Posted: 30 April 2019 doi:10.20944/preprints201904.0332.v1

Peer-reviewed version available at Appl. Sci. 2019, 9, 2190; doi:10.3390/app9112190

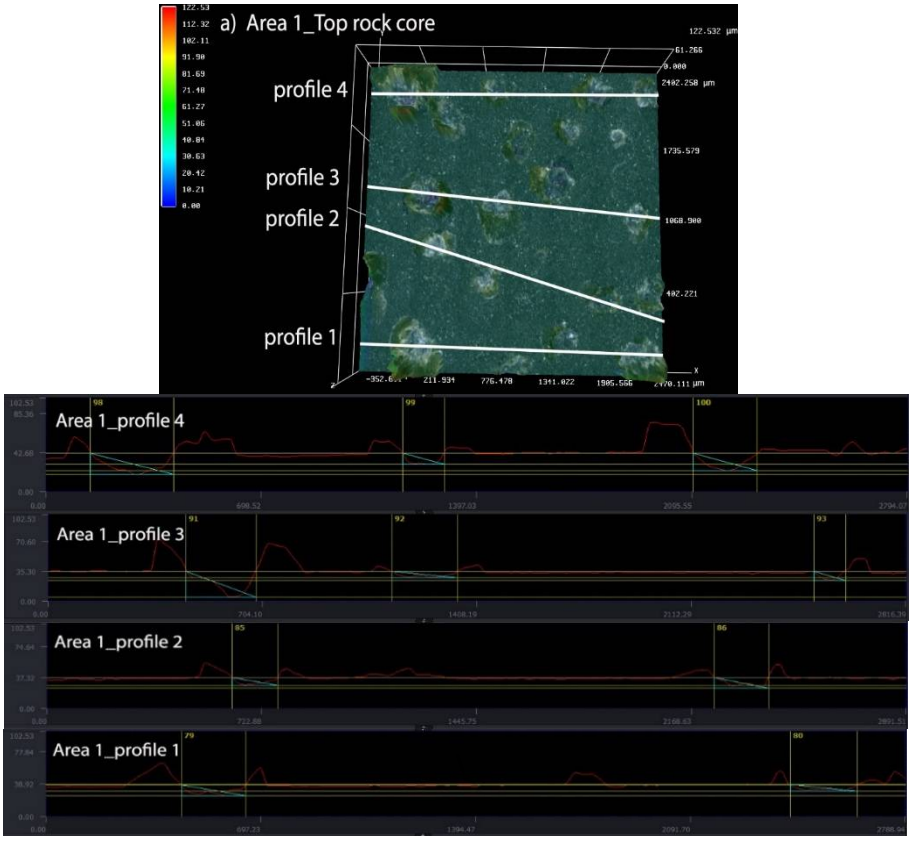

Figure 11. Average depth $H_{e_{T.a}}$ and average percentage surface damage $PDW_{e_{T.a}}$ for the top core plug (Test 1): (a) area 1

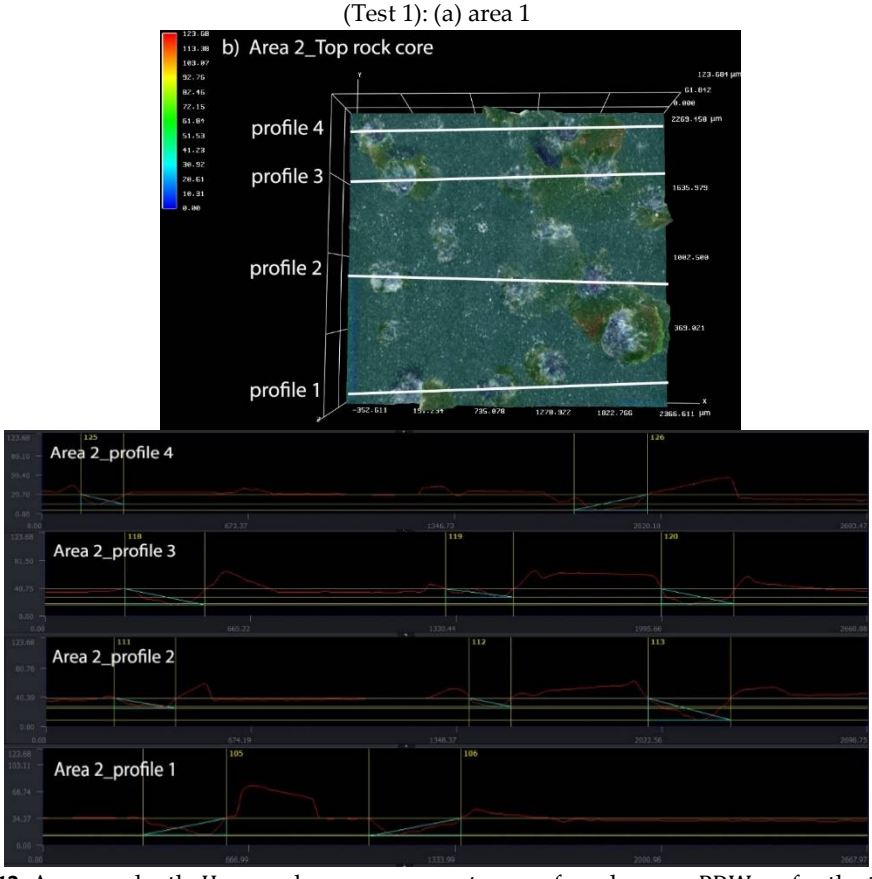

Figure 12. Average depth $H_{e_{T.a}}$ and average percentage surface damage $PDW_{e_{T.a}}$ for the top core plug (Test 1): (b) area 2

Peer-reviewed version available at Appl. Sci. 2019, 9, 2190; doi:10.3390/app9112190

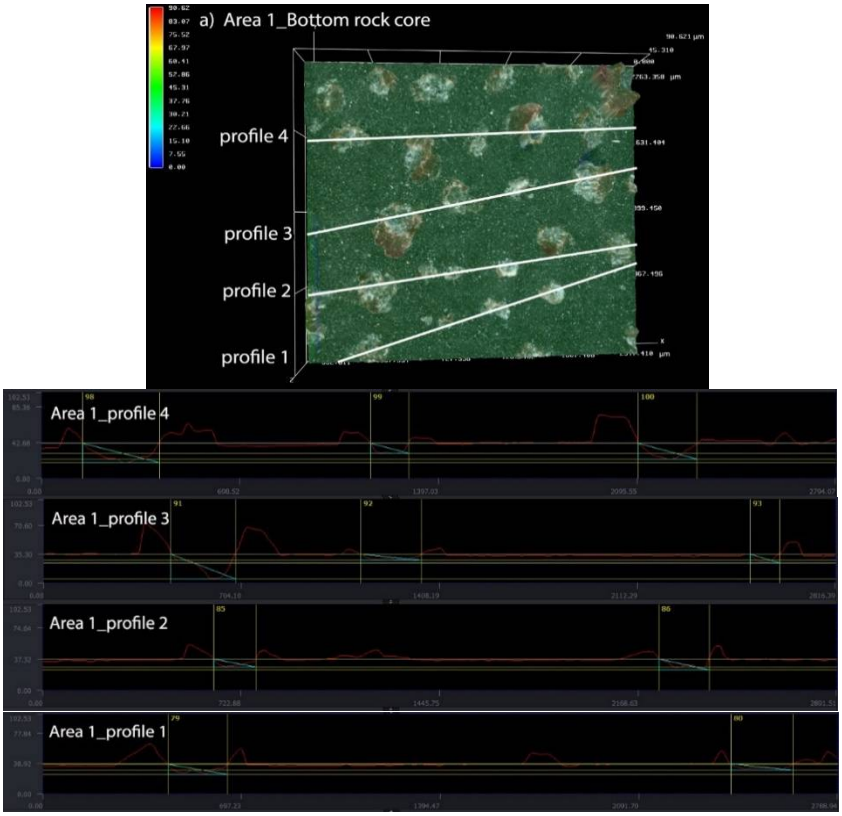

Figure 13. Average depth $H_{e_{B.a}}$ and average percentage surface damage $PDW_{e_{B.a}}$ for the bottom core plug (Test 1): (a) area 1.

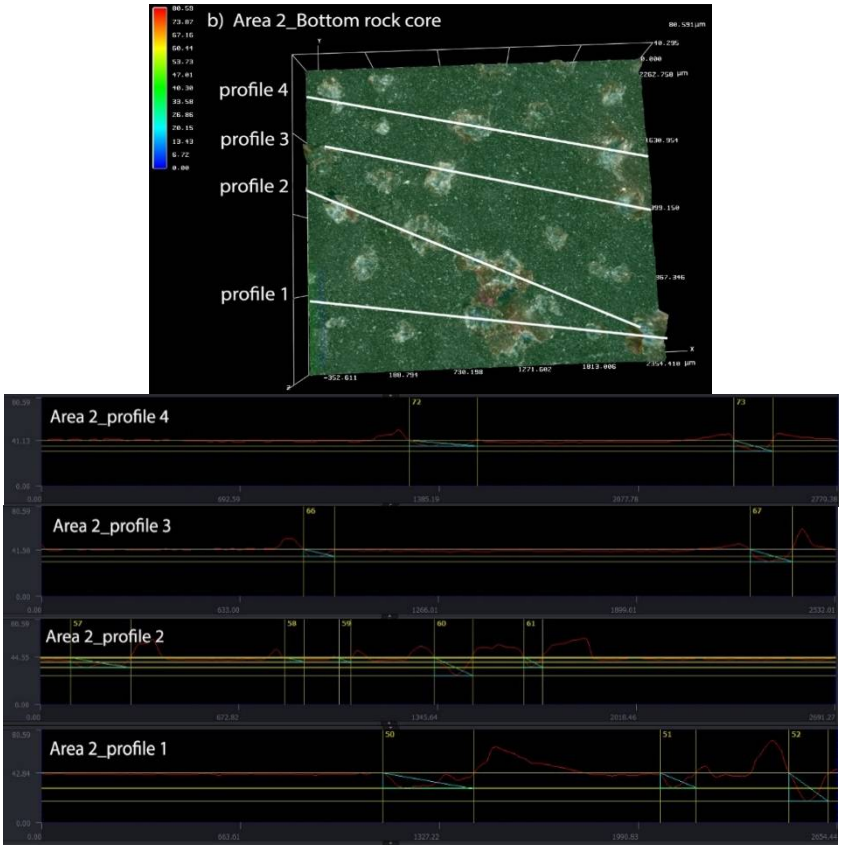

Figure 14. Average depth $\mathbf{H_{e_{B.a}}}$ and average percentage surface damage $\mathbf{PDW_{e_{B.a}}}$ for the bottom core plug (Test 1): (b) area 2

Peer-reviewed version available at Appl. Sci. 2019, 9, 2190; doi:10.3390/app9112190

Test no. 2 was performed in order to determine the maximum achievable width of the fracture packed with light ceramic proppant. The conditions of test no. 2 are presented in Table 1. In test no. 2 cylindrical core plugs were replaced with cylindrical steel plugs. After 6 hours of exposition to the defined axial compressive stress, a maximum fracture width W_{fm} of 1.514 mm was obtained.

The uncertainty of the estimated width of the fracture packed with proppant was determined based on the accuracy of the LVDT fracture gauge (+/- 0.001 mm). The uncertainty of the estimated total average depth of proppant embedding in the fracture faces is determined based on standard deviation from the average value. Effective fracture proppant packed parameters are presented in Figure 15.

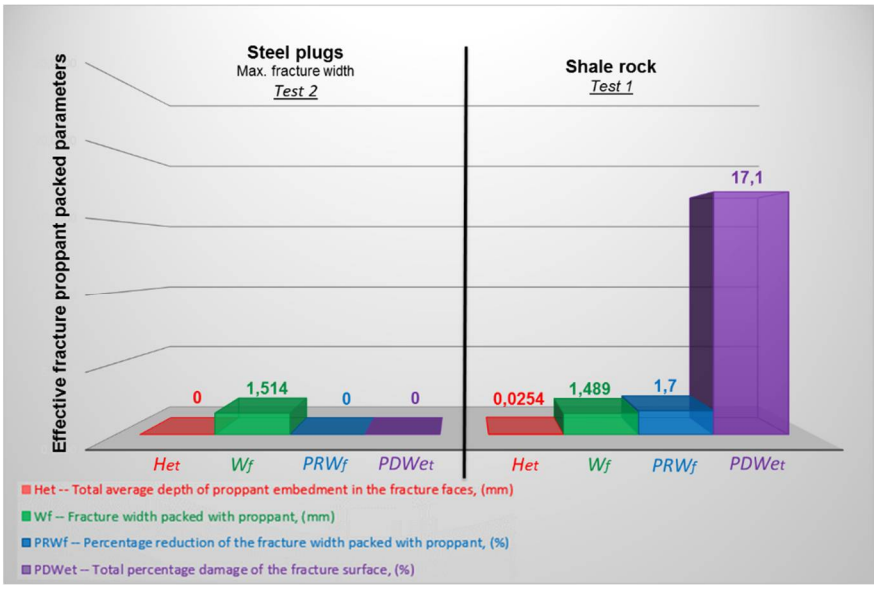

Figure 15. Effective packed fracture with the proppant for cylindrical steel plugs and shale rock

In addition, an attempt was made to simulate the effect of embedment on effective packed fracture with only one proppant layer. The maximum fracture width, corresponding to an average diameter of the tested proppant grains, amounting to 0.450 mm was used for the calculation. It was assumed that the value of average depth of proppant embedment He_t and surface damage $PDWe_t$, were equal to the values obtained in test no. 1. The results of this analysis are presented in Figure 16.

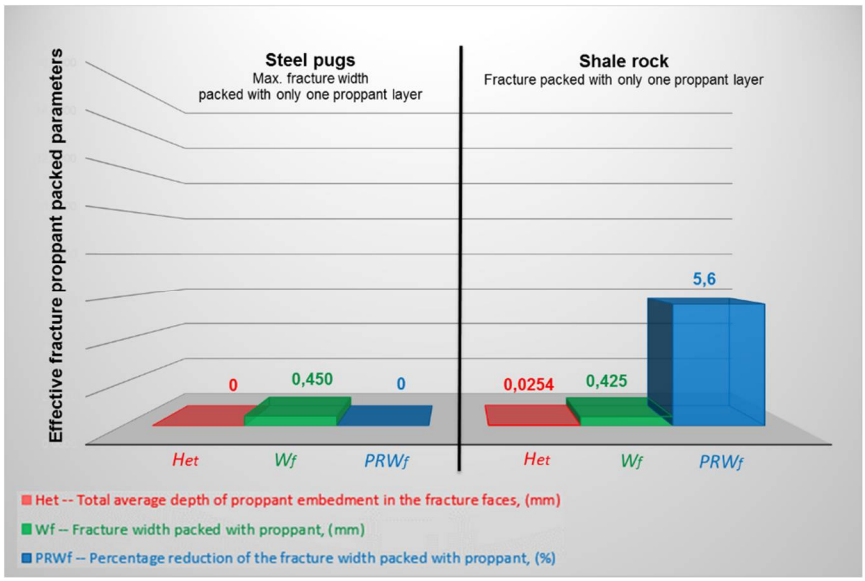

Figure 16. Effective packed fracture with the proppant for shale rock packed with one layer of proppant (grains size 0.600÷0.300 mm).

4. Discussion

Measurements are performed for a light ceramic proppant with 0.600÷0.300 mm grains size, low surface concentration of proppant 2.44 kg/m^2 and axial compression stress 48.3 MPa for 6 hours at 70 °C. The average diameter of the proppant grains is 0.450 mm. The tested dry shale rock is characterized by a slight damage to the surface of the fracture face by the embedment phenomenon, amounted to 17.1 %. The total depth of proppant embedment in the fracture faces is 0.0254 mm. The obtained width of the fracture is 1.489 mm, therefore 1.7 % less than the maximum achievable fracture width, which can be 1.514 mm, for the specified test conditions. For the additionally simulated maximum fracture width (0.450 mm), corresponding to only one layer of the tested proppant, the decrease of the maximum fracture width by 5.6 % is obtained. In this case, the depth of the proppant embedment of 0.0254 mm is used for the calculation. The final width of such packed fracture is 0.425 mm.

The size of the fracture width determines the flow of hydrocarbons from the reservoir to the wellbore. The tested dry shale rock allows to maintain width of packed fracture in order to flow of hydrocarbons.

Test results indicate that the developed method of measurement may be one of the preliminary assessment of the proper selection when choosing the proppant type and fracturing fluid for hydraulic fracturing of unconventional reservoirs, especially shale rocks.

Acknowledgements

This paper is based on the results from statutory work. Archive no. DK-4100-56/17.

References

[1] Economides, M.J.; Nolte K.G. Reservoir Stimulation. Second edition. Houston, **1989**.

[2] Chong, K.K.; Grieser, W.V.; Passman, A.; Tamayo, C.H.; Modeland, N.; Burke, B.. A completions Guide Book to Shale-Play Development: A Review of Successful Approaches Towards Shale-Play Stimulation in the Last Two Decades. *Paper Society of Petroleum Engineers presented at the Canadian Unconventional Resources and International Petroleum Conference*, 19-21 October **2010**, Calgary, Alberta, Canada. SPE 133874-MS. DOI: 10.2118/133874-MS

[3] Kasza, P. Stimulation treatments in unconventional hydrocarbon reservoirs. *Nafta-Gaz* **2011**, no. 10, pp. 697-701.

[4] Alramahi, B.; Sundberg, M. I. Proppant embedment and conductivity of hydraulic fractures in Shales. *American Rock Mechanics Association* **2012**, ARMA 12-291, pp. 1-6.

[5] Kasza, P.; Wilk, K. Completion of shale gas formations by hydraulic fracturing. *Przemysł Chemiczny* **2012**, no. 4, pp. 608-612.

[6] Masłowski, M. Studies of the conductivity of proppant material for the wet gas (nitrogen) after the hydraulic fracturing treatment of unconventional reservoirs. *Nafta-Gaz* **2016**, no. 3, pp. 177-185.

[7] Masłowski, M.; Biały, E.. Studies of the embedment phenomenon in stimulation treatments. *Nafta-Gaz* **2016**, no. 12, pp. 1101-1106. DOI: 10.18668/NG.2016.12.13

[8] King, G.E.; Apache Corporation: Thirty Years of Gas Shale Fracturing: What Have We Learned?. *Paper Society of Petroleum Engineers presented at the SPE Annual Technical Conference and Exhibition*, 19-22 September **2010**, Florence, Italy. SPE 133456-MS. DOI: 10.2118/133456-MS.

[9] Morales, H. Sustaining Fracture Area and Conductivity of Gas Shale Reservoirs for Enhancing Long-Term Production and Recovery. *RPSEA Unconventional Gas Conference* **2012**: Geology, the Environment, Hydraulic Fracturing, Canonsburg, 17-18.IV.2012.

[10] Masłowski, M.; Kasza, P.; Wilk K. Studies on the effect of the proppant embedment phenomenon on the effective packed fracture in shale rock. *Acta Geodynamica et Geomaterialia* **2018**, Vol. 15, No. 2 (190), pp. 105-115. DOI: 10.13168/AGG.2018.0012.

[11] Beckmann, G.; Retsch Technology GmbH Measuring the Size and Shape of Frac Sand and other Proppants. *Webinar Presentation*, 09.03.**2012**.

[12] Masłowski, M. Proppant material for hydraulic fracturing in unconventional reservoirs. *Nafta-Gaz* **2014**, no. 2, pp. 75-86.

[13] Mueller, M.; Amro, M. Indentaion Hardness for Improved Proppant Embedment Prediction in Shale Formation. *Paper Society of Petroleum Engineers presented at the SPE European Formation Damage Conference and Exhibition*, 3-5 June **2015**, Budapest, Hungary. SPE 174227-MS. DOI: 10.2118/174227-MS

[14] Handren, P.; Palisch, T. Successful Hybrid Slickwater Fracture Design Evolution – An East Texas Cotton Valley Taylor Case History. *Paper Society of Petroleum Engineers presented at the SPE Annual Technical Conference and Exhibition*, 11-14 November **2007**, Anaheim, California, U.S.A. SPE 110451-MS. DOI: 10.2118/110451-MS

[15] Volk, L.J.; Raible, C.J.; Carrol, H.B.; Spears, J.S.: Embedment of high strength proppant into low-permeability reservoir rock. *Paper Society of Petroleum Engineers presented at the SPE/DOE Low Permeability Gas Reservoirs Symposium*, 27-29 May **1981**, Denver, Colorado. SPE 9867-MS. DOI: 10.2118/9867-MS

[16] Zhang, J.; Ouyang, L.; Hill, A.D.; Zhu, D.: Experimental and Numerical Studies of Reduced Fracture Conductivity due to Proppant Embedment in Shale Reservoirs. *Paper Society of Petroleum Engineers presented at the PE Annual Technical Conference and Exhibition*, 27-29 October **2014**, Amsterdam, The Netherlands. SPE 170775-MS, pp. 1-15. DOI: 10.2118/170775-MS

[17] Sato, K.; Wright, Ch.; Ichikawa, M. Post-Frac analysis indicating multiple fractures created in a volcanic formation. *Paper Society of Petroleum Engineers presented at the SPE India Oil and Gas Conference and Exhibition*, 17-19 February **1998**, New Delhi, India . SPE 39513-MS. DOI: 10.2118/39513-MS

[18] Legarth, B.; Huenges, E.; Zimmermann, G. Hydraulic fracturing in a sedimentary geothermal reservoir: Results and implications. *International Journal of Rock Mechanics & Mining Sciences* 42, 28.VI.**2005**; pp. 1028–1041.

[19] Masłowski, M. Studies of the embedment phenomenon after the hydraulic fracturing treatment of unconventional reservoirs. *Nafta-Gaz* **2015**, no. 7, pp. 461-471.

[20] Masłowski, M.; Kasza, P.; Czupski, M. Studies of the susceptibility of the tight gas rock to the phenomenon of embedment, limiting the effectiveness of hydraulic fracturing. *Nafta-Gaz* **2016**, no. 10, pp. 822-832. DOI: 10.18668/NG.2016.10.07.

[21] Ghassemi, A.; Suarez-Rivera, R. Sustaining Fracture Area and Conductivity of Gas Shale Reservoirs for Enhancing Long-Term Production and Recovery. *Research Partnership to Secure Energy for America. Final report of Project*, no. 08122-48, 15.V.**2012**.

[22] Guo, J.; Liu, Y. Modeling of Proppant Embedment: Elastic Deformation and Creep Deformation. *Paper Society of Petroleum Engineers presented at the SPE International Production and Operations Conference and Exhibition*, Doha, Qatar, 14-16 May **2012**. SPE 157449-MS. DOI: 10.2118/157449-MS

[23] Zhang, F.; Zhu, H.; Zhou, H.; Guo, J.; Bo, H. Discrete-Element-Method/Computational-Fluid-Dynamics Coupling Simulation od Proppant Embedment and Fracture Conductivity After Hydraulic Fracturing. *SPE Journal*, volume 22, 04.**2017**; pp. 632-644. SPE 185172-PA. DOI:10.2118/185172-PA

[24] Masłowski, M.; Kasza, P.; Czupski, M.; Wilk, K. Sposób wyznaczania zmniejszenia rozwartości podsadzonej szczeliny, *Urząd Patentowy RP.* Patent nr 228609; 10.04.**2018**.

[25] Ghassemi, A.; Suarez-Rivera, R. Sustaining Fracture Area and Conductivity of Gas Shale Reservoirs for Enhancing Long-Term Production and Recovery. Appendix 5 – Proppant Embedment Standard Testing Procedure. *Research Partnership to Secure Energy for America*. Final report of Project no. 08122-48. 15.V.**2012**.

[26] PN-EN ISO 13503-5: „Przemysł naftowy i gazowniczy – Materiały i płyny do dowiercania złóż – Część 5: Procedury pomiaru długotrwałej przewodności materiałów podsadzkowych (ISO 13503-5:2006)". *Polski Komitet Normalizacyjny*, Warszawa, wrzesień **2009**.